Fundamental and Random Birefringence Limitations to Delay in Slow Light Fiber Parametric Amplification

Luca Schenato, *Member, IEEE*, Marco Santagiustina, *Member, IEEE*, and Carlo G. Someda, *Senior Member, IEEE*

***Abstract*—Narrowband fiber parametric amplification is known to provide slow and fast light capabilities. Here, an analytical expression of the maximum slow light time delay achievable in ideal, isotropic fibers is derived. Then, the effects of random birefringence on the slow and fast light ability are numerically investigated by integrating the governing equations over a large number of statistical realizations of the fiber. The different polarization rotation along the fiber for the signal, the idler, and the pump reduces the amplifier mean gain and the mean time delay. For small random birefringence, the decrease of the mean delay can be directly imputed to the reduction of the mean gain. For large random birefringence, severe pulse distortion occurs, the mean delay is further reduced and the delay uncertainty highly enhanced. The influence of the stimulated Raman scattering is finally addressed.**

***Index Terms*—Optical fiber amplifiers, optical fiber dispersion, optical fiber polarization, Raman scattering.**

I. Introduction

NARROWBAND optical parametric amplifiers (NB-OPAs), originally envisaged as general purpose fiber optic amplifiers [1], have spurred interesting applications in the field of all-optical signal processing. In particular, the large group delay tuning capability that characterizes the NB-OPA makes it a suitable candidate for slow and fast light (SFL) optical delay lines [2]–[4]. However, recent experiments and preliminary theoretical analysis showed that NB-OPA gain and delay can be severely affected by fiber impairments, like the random variation of the fiber birefringence and the fluctuation of the zero dispersion wavelength (ZDW) [5]–[8].

In this work, attention is focused on the random birefringence [7], [9] which mainly causes a different evolution of the state of polarization (SOP) of the pump, signal and idler waves, determining a random variation of the gain and of the time delay.

Here, the influence of random birefringence on pulse delay is studied through a statistical approach, in which hundreds of different realizations of the random birefringence are calculated, to explore in detail the tolerance of SFL NB-OPA schemes. First, in Section II, the equations that govern NB-OPA are introduced and an exact analytical expression for the maximum delay that can be attained without birefringence is provided. In Section III, the time delay and gain when random birefringence is also taken into account are investigated numerically. In Section IV, the numerical analysis is extended to consider the effects of the stimulated Raman scattering (SRS). Finally, the conclusions are summarized in Section V.

Manuscript received April 15, 2008; revised August 12, 2008. Current version published January 28, 2009. This work, held in agreement with ISCOM (Rome), was supported by the Italian and Korean Republics Governments under Project "Special optical fibers and devices for photonics applications in communications and sensing." The work of L. Schenato was supported by the University of Padua under Grant "Optical fiber for slow and fast light applications" (CPDR065915).

The authors are with the Department of Information Engineering, University of Padova, 35131 Padova, Italy (e-mail: luca.schenato@dei.unipd.it).

Digital Object Identifier 10.1109/JLT.2008.2004970

II. Maximum Delay in Isotropic Fibers

Let us consider the parametric interaction of three electric fields $E_m(z,t) = |A_m(z)\rangle \exp\{\jmath[k_m z - \omega_m t]\}, m = p, s$ or i, where $|A_p, |A_s\rangle, |A_i\rangle$ are the complex Jones vectors of the pump, the signal, and the idler, respectively, at the optical frequencies ω_p, ω_s and ω_i satisfying $2\omega_p = \omega_s + \omega_i$. The propagation constants are $k_m = k(\omega_m), m = p, s, i$. The equations used to describe the propagation of the Jones vectors in an OPA are those obtained in the undepleted pump approximation and neglecting losses and the nonlinear effects of the signal and idler on the pump [6], [10]:

$$\begin{aligned} \partial_z |A_p\rangle &= (\mathcal{L}_p + \mathcal{S}_p)|A_p\rangle \\ \partial_z |A_{s,i} &= (\mathcal{L}_{s,i} + \mathcal{X}_p + \mathcal{R}_{s,i})|A_{s,i}\rangle + \mathcal{F}_{s,i}|A_{i,s}\rangle. \end{aligned} \quad (1)$$

Through proper operators, the model takes into account the nonlinear induced modulation (self-phase $\mathcal{S}_p$, cross-phase $\mathcal{X}_p$), the parametric $(\mathcal{F}_{s,i})$ and Raman $(\mathcal{R}_{s,i})$ interaction, where for the latter the extended model of [11] was used. The linear operators $(\mathcal{L}_{p,s,i})$ also depend on the random birefringence Stokes vector $\vec{\beta}(\omega)$ [10].

For initially linear, co-polarized fields and when no birefringence is considered the waves maintain the same SOPs for the entire propagation. In this case, the evolution of the wave envelopes are represented by scalar quantities; the pump is simply $A_p(z) = \sqrt{P_0}\exp(\jmath\gamma P_0 z)$ while the signal and the idler are governed by two coupled equations [2]:

$$\frac{\partial A_{s,i}}{\partial z} = \jmath 2\gamma P_0 A_{s,i} + \jmath\gamma P_0 A_{i,s}^* \mathrm{e}^{\jmath(2\gamma P_0 - \Delta k)z} \quad (2)$$

where γ is the fiber nonlinear coefficient and $\Delta k = k_i + k_s - 2k_p$ is the linear phase mismatch between the propagation constants.

Equation (2) has an analytical solution, and it can be shown that substantial amplification occurs for $-4\gamma P_0 < \Delta k < 0$ [12]. By defining the nonlinear length $L_{\mathrm{NL}} = (\gamma P_0)^{-1}$, the maximum signal gain is

$$G_s = 1 + \sinh^2\left(\frac{L}{L_{\mathrm{NL}}}\right) \quad (3)$$

which is found for $\Delta k = -2\gamma P_0 = -2/L_{\mathrm{NL}}$.

The SFL delay can be determined once the gain spectrum, i.e., the fiber dispersion properties, has been defined. Here, the

0733-8724/$25.00 © 2008 IEEE

fiber dispersion is modeled through a Taylor expansion around the pump frequency ω_p up to the fourth order. Then, $\Delta k = k_2(\omega_s - \omega_p)^2 + k_4(\omega_s - \omega_p)^4/12$, where k_n is the nth angular frequency derivative of $k(\omega)$, evaluated at ω_p [2], [13]. The third-order dispersion term k_3 does not appear in the expression of Δk due to the fact that $\omega_s - \omega_p = -(\omega_i - \omega_p)$, yielding the third-order terms of k_s and k_i to have opposite sign and to cancel out. By varying the pump wavelength in the proximity of the ZDW, λ_0, k_2 can be tuned over a wide range of values, because $k_2 \approx \partial^3 k/\partial\omega^3(\omega_0)(\omega_p - \omega_0) + 1/2\partial^4 k/\partial\omega^4(\omega_0)(\omega_p - \omega_0)^2$, where $\omega_0 = 2\pi c_0/\lambda_0$, where c_0 is the speed of light in the vacuum. Moreover, when ω_p is close to ω_0 in the normal dispersion regime (i.e., $k_2 > 0$), the nonlinear matching conditions can be satisfied only for $k_4 < 0$ and far from the pump frequency, in two well separated narrow spectral bands, symmetric with respect to ω_p. For the purpose of the discussion, we will assume that the signal is at shorter wavelengths whereas the idler is at longer wavelengths. Due to the gain narrowing the group index increases [decreases] at shorter wavelength, and the signal [idler] is slowed down [advanced].

Note that the reduced equations considered in this section do not take into account the SRS. The SRS has an effect on the gain, but it also modifies the group delay via the gain spectral shape. However, when the signal and idler detuning from the pump wavelength is large enough (more than 120 nm), the effects of the SRS gain are negligible [2]. So, here and in Section III, the SRS is not considered, assuming a large detuning and under this approximation an exact formula for the delay can be determined. The analytical result, confirmed by numerical solutions, is then exploited to quantify the effects which random birefringence and SRS exert on SFL propagation in the following sections.

The analytical expression of the group index [2] over the entire gain bandwidth enables the calculation of an analytical expression for the signal time delay (and of the idler time advance) ΔT at all frequencies. The formula is reported in the Appendix, for the sake of brevity. At phase matching ($\Delta k = -2/L_{\rm NL}$), the delay is given by

$$\Delta T = L\sqrt{6k_2}\sqrt{\frac{1}{L_{\rm disp}}}\sqrt{1+\frac{2}{3}\frac{L_{\rm disp}}{L_{\rm NL}}} \times \sqrt{1+\sqrt{1+\frac{2}{3}\frac{L_{\rm disp}}{L_{\rm NL}}}}\left[1-\frac{L_{\rm NL}}{L}\tanh\left(\frac{L}{L_{\rm NL}}\right)\right] \quad (4)$$

where $L_{\rm disp} = -k_4/k_2^2$ is a length scale that depends on the fiber dispersion. Note that the value of $L_{\rm disp}$ is fixed by the fiber, whereas the nonlinear length $L_{\rm NL}$ also depends on the injected power P_0. Dispersion-shifted fibers (DSF) that could be used for SFL have typically $L_{\rm disp}$ of the order of few meters, whereas the nonlinear length varies from some hundreds meters down to some meters when the pump power is in the order of some watts. As an example, let us consider a DSF with $\gamma = 2.3\,{\rm W}^{-1}{\rm km}^{-1}$, ZDW $\lambda_0 = 1542.3$ nm, $k_3(\lambda_0) = 1.14 \times 10^{-40}\,{\rm s}^3{\rm m}^{-1}$ and $k_4(\lambda_0) = -5 \times 10^{-55}\,{\rm s}^4{\rm m}^{-1}$. The delay ΔT as a function of $L_{\rm NL}/L_{\rm disp}$ and normalized with respect to

$$\Delta T_0 = L\sqrt{12k_2}\sqrt{\frac{1}{L_{\rm disp}}} \quad (5)$$

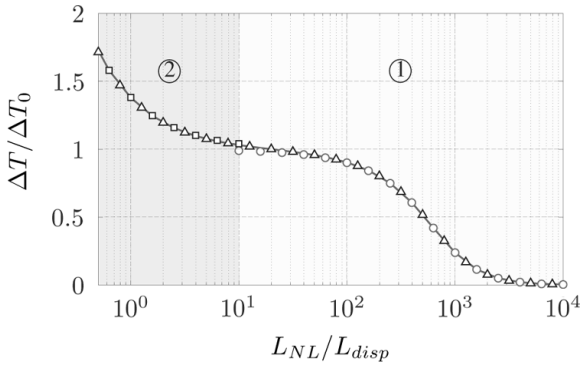

Fig. 1. $\Delta T/\Delta T_0$ versus $L_{\rm NL}/L_{\rm disp}$ when $L = 1000\,L_{\rm disp}$. The continuous line is obtained from (4); the triangles are the result of the numerical integrations of the (2); the empty circles [squares] are calculated with (6) [(7)] that provides an excellent approximation when $L_{\rm NL} \gg L_{\rm disp}[L_{\rm NL} \simeq L_{\rm disp}]$ (region ①) [(region ②)].

is represented by the continuous curve of Fig. 1 for a fiber whose length is $L = 1000 L_{\rm disp}$. In the same figure, the triangles are obtained by numerical integration of (2) by means of a split-step, Fourier, beam propagation method. The agreement is excellent (in the order of the machine precision).

Depending on the relative magnitude of L, $L_{\rm disp}$ and $L_{\rm NL}$, there exist two different regimes.

When $L_{\rm NL} \gg L_{\rm disp}$ (low powers for which the dispersive effects are still dominant corresponding to the region ①of Fig. 1) (4) can be approximated by

$$\Delta T \simeq \Delta T_0 \left[1 - \frac{L_{\rm NL}}{L}\tanh\left(\frac{L}{L_{\rm NL}}\right)\right]. \quad (6)$$

Equation (6) is represented by the empty circles in Fig. 1. In this regime ΔT_0 represents an upper bound for the maximum achievable delay $\forall L$.

When $L_{\rm NL} \simeq L_{\rm disp}$ (region ②of Fig. 1) nonlinear effects highly contribute to determine the delay; this is the regime of highly nonlinear fibers. In this case, the expression for ΔT reads

$$\Delta T \simeq \Delta T_0 \left(\frac{1}{\sqrt{2}}\sqrt{1+\frac{2}{3}\frac{L_{\rm disp}}{L_{\rm NL}}}\sqrt{1+\sqrt{1+\frac{2}{3}\frac{L_{\rm disp}}{L_{\rm NL}}}}\right). \quad (7)$$

Equation (7) is represented by empty squares in Fig. 1. Note that the regime for which $L_{\rm NL} < L_{\rm disp}$ would occur for extremely large value of P_0, for which the undepleted pump assumption does not hold any longer. In that case pump depletion saturates the gain and the delay. So, the analysis reveals that in practical cases there exists a maximum achievable delay which is close to ΔT_0. So, the maximum delay depends only on the fiber dispersion parameters and on the detuning $\lambda_0 - \lambda_p$ between the ZDW and the pump wavelength, which sets k_2 (and thus $L_{\rm disp}$).

The exact formula (4), confirmed by the numerical simulations, enables one to determine ΔT as a function of the ZDW-pump detuning, without the need for extensive computer integrations. The contour plots of ΔT are represented in Fig. 2 for the same fiber, but 1 km long, as a function of $\lambda_0 - \lambda_p$ and $1/L_{\rm NL}$. Large delays are shown as brighter areas.

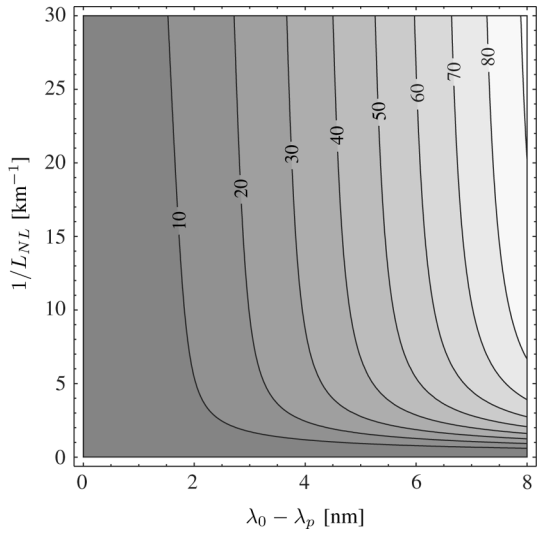

Fig. 2. Contour plot of ΔT [ps] versus $1/L_{\rm NL}$ [km^{-1}] and $\lambda_0 - \lambda_p$ [nm]: bright areas correspond to larger delays.

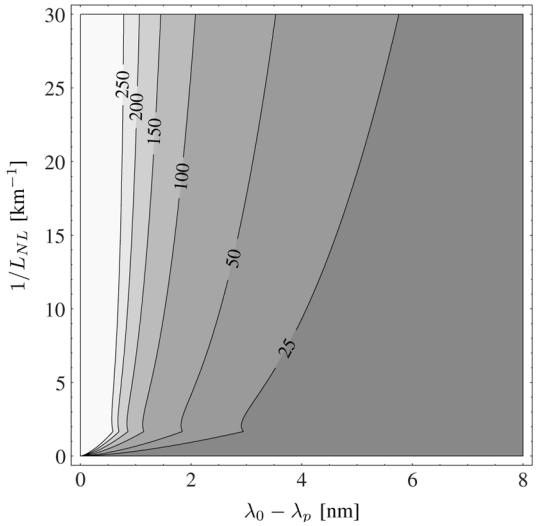

Fig. 3. Contour plot of B [GHz] versus $1/L_{\rm NL}$ [km^{-1}] and $\lambda_0 - \lambda_p$ [nm]: bright areas correspond to wider OPA gain bandwidth.

Note that the delay can be highly increased by widening the detuning by a few nanometers. However, the gain bandwidth B, defined here as the minimum between the full-width at half-maximum (FWHM) bandwidth, $B_{3\,\rm dB}$, and the bandwidth for which $-4\gamma P_0 < \Delta k < 0$, where the gain is "substantial" [1], is correspondingly reduced, as shown in the contour plot of Fig. 3. Please note that the maximum gain is $1 + [\sinh(L/L_{\rm NL})]^2$ and for $-4\gamma P_0 < \Delta k < 0$ the gain is always larger than $1 + (L/L_{\rm NL})^2$; when $L/L_{\rm NL}$ is smaller than ~ 1.67, $1 + (L/L_{\rm NL})^2 \geq \{1 + [\sinh(L/L_{\rm NL})]^2\}/2$ and the FWHM bandwidth, $B_{3\,\rm dB}$, becomes larger than the bandwidth for which $-4\gamma P_0 < \Delta k < 0$. Consequentially, the bandwidth represented in Fig. 3 for $L/L_{\rm NL} \geq 1.67$ corresponds to the FWHM bandwidth, $B_{3\,\rm dB}$, whereas when $L/L_{\rm NL} < 1.67$ it corresponds to the bandwidth defined in [1]. The explanation for the concomitant increasing of the delay in presence of a reduction of the bandwidth is very clear: by increasing the detuning the delay grows because the gain bandwidth narrows, i.e., changes rapidly with the frequency. So, if the bandwidth delay product $B \times \Delta T$ is considered as a figure of merit, there is no advantage in increasing the detuning $\lambda_0 - \lambda_p$, as shown by the almost horizontal contour plots of Fig. 4.

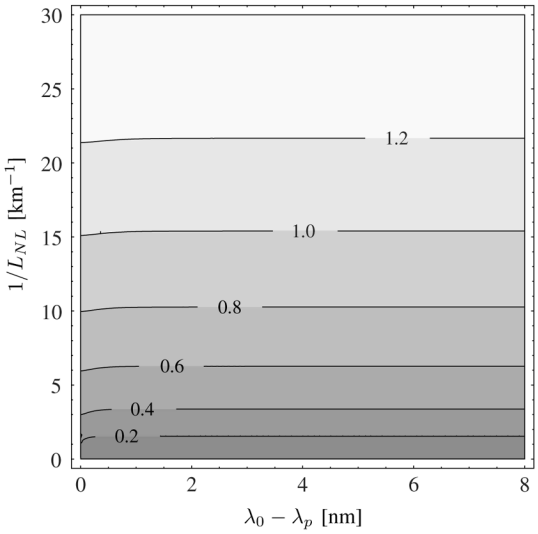

Fig. 4. Contour plot of the figure of merit $B \times \Delta T$ versus $1/L_{\rm NL}$ [km^{-1}] and $\lambda_0 - \lambda_p$ [nm]: bright areas correspond to larger values of the figure of merit.

III. Random Birefringence Effects

In real fibers, the SOPs of the three waves change randomly over the entire fiber because of the effects of the random birefringence. Then a reduction of the mean gain and of the mean time delay can be expected and they are numerically investigated here.

The fiber considered has the same parameters used in the previous section, with $L = 1$ km. The birefringence along the fiber is modeled by a cascade of constant birefringence sections [14]; two different mean PMD-coefficients, D_p [ps/$\sqrt{\rm km}$], have been considered $D_p = 0.025$ and $0.08\,{\rm ps}/\sqrt{\rm km}$. A statistical ensemble of some hundreds of fiber realizations for each of the two mean PMD-coefficients have been generated and (1) has been numerically integrated. Then, the mean values and the standard deviations (STD) of the gain and of the delay for each D_p and for different pump power levels and linearly co-polarized input SOPs, have been calculated separately. It is important to note that when random birefringence is present the signal is also distorted by the polarization mode dispersion [15]. For this reason, though the gain is calculated for each realization at ω_s satisfying $\Delta k = -2\gamma P_0$, the delay has been measured with respect to the first moment of time for the pulse, as defined in [16].

The pump is a continuous wave at $\lambda_p = 1535$ nm, whereas the signal is a 70-ps FWHM Gaussian pulse. The pump power P_0 was varied in the range from 0 to 9 W with a step of 0.5 W and the signal power at the input was -40 dBm. Note that the pump wavelength and power were chosen so as to have $\lambda_p - \lambda_s \sim 150$ nm, i.e., a detuning that minimize the SRS effects. Correspondingly, $L_{\rm disp} \approx 1.17$ m and $L_{\rm NL}$ is always larger than 48 m. Then, if the birefringence was not present, the delay would

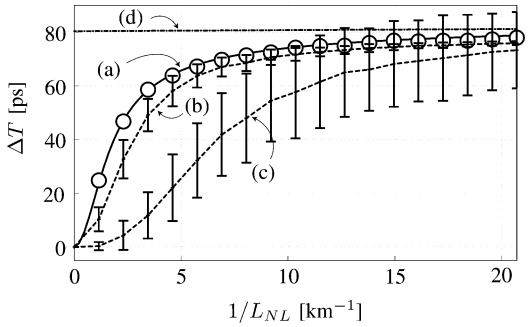

Fig. 5. Time delay versus $1/L_{\rm NL}$. The continuous line (a) is calculated from (4); the empty circles are the numerical results obtained for $D_p = 0$. Curves (b) and (c) are the numerical results for $D_p = 0.025\,\text{ps}/\sqrt{\text{km}}$ and $D_p = 0.08\,\text{ps}/\sqrt{\text{km}}$, respectively; (d) is ΔT_0.

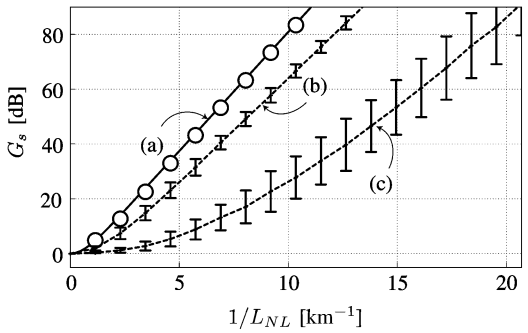

Fig. 6. Signal gain versus $1/L_{\rm NL}$. The continuous line (a) is calculated from (3); the empty circles are numerical results for $D_p = 0$. Curves (b) and (c) are the numerical results for $D_p = 0.025\,\text{ps}/\sqrt{\text{km}}$ and $D_p = 0.08\,\text{ps}/\sqrt{\text{km}}$, respectively.

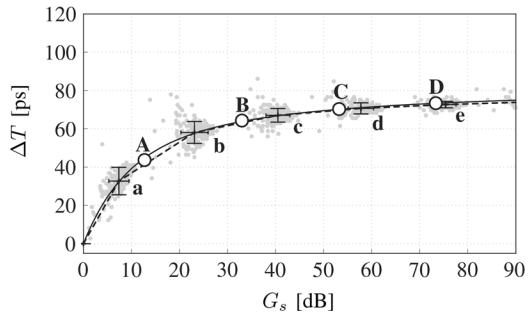

Fig. 7. Plot of the time delay versus signal gain. The continuous line is the theoretical solution ((3) and (4)) while the empty circles $(\mathrm{A}, \mathrm{B}, \ldots)$ are the numerical values calculated with no birefringence $(D_p = 0)$ for $P_0 = 1, 2 \cdots 5$ W. The dots represent single realizations for $D_p = 0.025\,\text{ps}/\sqrt{\text{km}}$. Letters $(\mathrm{a}, \mathrm{b}, \ldots)$ refer to the same values of P_0; the gain-delay means have been plotted with their STDs represented by the bars.

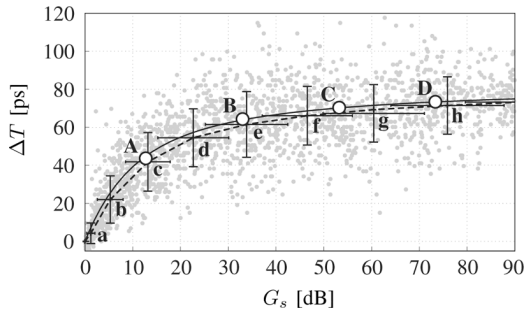

Fig. 8. Plot of the time delay versus signal gain. The continuous line is the theoretical solution ((3) and (4)) while the empty circles $(\mathrm{A}, \mathrm{B}, \ldots)$ are the numerical values calculated with no birefringence $(D_p = 0)$ for $P_0 = 1, 2 \cdots 5$ W. The dots represent single realizations for $D_p = 0.08\,\text{ps}/\sqrt{\text{km}}$. Letters $(\mathrm{a}, \mathrm{b}, \ldots)$ refer to the same values of P_0; the gain-delay means have been plotted with their STDs represented by the bars.

be given by (6) for large $L_{\rm NL}$ (i.e., for small P_0) reaching the value ΔT_0 by decreasing $L_{\rm NL}$ (i.e., for large P_0).

The gain and the delay curves predicted by (3) and (4) are represented by the continuous curves (a) of Figs. 5 and 6, respectively. The empty circles are obtained numerically for $D_p = 0$ by integrating the full vectorial equations; the agreement is excellent both for the gain and for the delay. For $D_p = 0$, the maximum power to consider valid the undepleted pump approximation is ~ 4.5 W $(1/L_{\rm NL} \approx 10\ \text{km}^{-1})$, which yields a gain of about 72 dB. Nonetheless, Figs. 5 and 6 shows the numerical and analytical calculation of the delay and gain even for shorter nonlinear lengths. This is done to allow the comparison with the case when birefringence is present and the efficiency of the OPA interaction is decreased. Note, in fact, that the curves in presence of birefringence attain the same gain at smaller $L_{\rm NL}$ (higher pump powers). The dot-dashed curve (d) of Fig. 5 represents ΔT_0: as previously discussed $\Delta T \to \Delta T_0$ and the delay growth saturates before the gain saturation occurs.

In Figs. 5 and 6, the mean delay and gain, calculated over the two statistical ensembles, are represented as a function of $1/L_{\rm NL}$. The dashed curves (b) and (c) of Fig. 5, respectively, refer to the mean delay when $D_p = 0.025\,\text{ps}/\sqrt{\text{km}}$ and $D_p = 0.08\,\text{ps}/\sqrt{\text{km}}$. The STDs are represented by the vertical bars; note the very large uncertainty for curve (c); this is the most detrimental effect of random birefringence. In fact, the mean delay value is also reduced by the random birefringence but this effect could be compensated by decreasing $L_{\rm NL}$.

Analogously, in Fig. 6, the dash curves labeled (b) and (c) represent the gain respectively for $D_p = 0.025\,\text{ps}/\sqrt{\text{km}}$ and $D_p = 0.08\,\text{ps}/\sqrt{\text{km}}$, with the vertical bars representing the STDs. The results confirm that even for a small value of the PMD coefficient, the mean gain sensibly decreases and its standard deviation increases. Though affected by the PMD the gain (expressed in dB) grows almost linearly with $L_{\rm NL}^{-1}$ (and hence with P_0), though PMD decreases the OPA efficiency from 20 dB/W $(D_p = 0)$ down to about 11.15 dB/W $(D_p = 0.08\,\text{ps}/\sqrt{\text{km}})$.

In Figs. 7 and 8 the delay versus gain relation is shown, respectively, for $D_p = 0.025\,\text{ps}/\sqrt{\text{km}}$ and $D_p = 0.08\,\text{ps}/\sqrt{\text{km}}$ for the entire statistical ensembles (dots). The gain-delay mean values obtained by averaging over the ensembles (indicated by small letters) are joined by the dashed curves and the STDs are represented by vertical and horizontal bars. In the figures the theoretical curves with no birefringence given by (3) and (4) are also plotted (continuous curves) as well as the numerical results for the same condition (empty circles). Capital letters indicate the value P_0 used for $D_p = 0$, which matches that for the corresponding small letters used for $D_p \neq 0$.

Note that the mean gain-delay curve (dashed curve) in Fig. 7 is practically overlapped to the zero birefringence theoretical curve (continuous curve). The mean gain-delay values for a given P_0 (a, b, c, and d) are actually shifted, along the theoretical curve, with respect to the corresponding values for $D_p =$

0 (empty circles A, B, C, and D). This means that, for small PMD, the reduction of the delay can be imputed directly to the reduction of the gain. However, as shown in Fig. 8, if D_p grows the NB-OPA mean performance curve is found below the theoretical no-birefringence curve. Therefore, the reduction of time delay cannot be simply imputed to the relative reduction of the gain; actually severe pulse distortion is observed in those cases. Finally, note the large spread (STD) for $D_p = 0.08\,\mathrm{ps}/\sqrt{\mathrm{km}}$; the exploitation of similar fibers as a tunable delay line is practically impossible because of the large uncertainty in the delay and the strong pulse distortion. Such a large sensitivity of NB-OPA to random birefringence is due to the very narrowband of the gain and to the large frequency shift between the signal, the pump and the idler that are intrinsic peculiarities of this SFL scheme that is different from the wideband OPA [10].

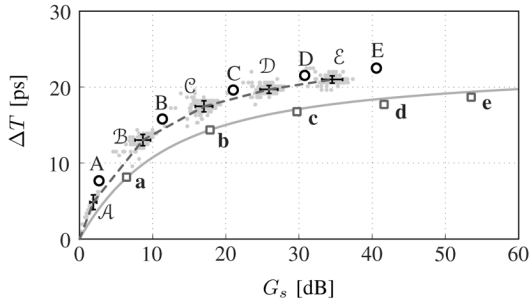

Fig. 9. Plot of the time delay versus signal gain. The continuous line is the theoretical solution [(3) and (4)] while the empty squares $(\mathrm{a}, \mathrm{b}, \ldots)$ are the numerical values calculated with no birefringence ($D_p = 0$) for $P_0 = 1, 2 \cdots 5$ W. The empty circles are the numerical results for $D_p = 0$ with SRS ($\mathrm{A}, \mathrm{B}, \ldots$ corresponding to $P_0 = 1, 2 \ldots 5$ W). The dots represent single realizations for $D_p = 0.025\,\mathrm{ps}/\sqrt{\mathrm{km}}$ and including the SRS ($\mathcal{A}, \mathcal{B} \cdots$ corresponding to $P_0 = 1, 2 \cdots 5$ W).

IV. Raman-Assisted NB-OPA With Random Birefringence

So far, the effects of the SRS on SFL OPA have been neglected, under the hypothesis that the signal-pump shift was large enough. SRS is accounted for here, by using the full model reported in [11], where the frequency shift dependent real and imaginary parts of the Raman response, for the parallel and orthogonal waves, are considered.

The imaginary part of the complex Raman response can be expected to induce absorption on the signal. However, it has been shown [17] that, at phase matching ($\Delta k = -2\gamma P_0$), the real part becomes relevant in reducing the OPA gain, whereas the imaginary part does not play a significant role. This can be explained by the fact that SRS changes the effective nonlinear coefficient. In fact, the real part of the Raman response adds to the nonlinear Kerr coefficient and the delay is finally increased [2].

In Fig. 9, the delay versus gain curve is plotted for a 600-m-long fiber with the same parameters of the previous sections. The pump wavelength is 1538 nm: for $P_0 = 0, 1, \ldots 5$ W, the signal wavelength $\lambda_s \simeq 1426$ nm is close to the negative peak of the real part of the Raman response. Since large values of D_p introduce severe distortions, only the case of small PMD coefficient ($D_p = 0.025\,\mathrm{ps}/\sqrt{\mathrm{km}}$) is considered here for the sake of clarifying the effects of SRS.

The theoretical curve for $D_p = 0$ and no SRS [(3) and (4)] is plotted as a continuous gray curve; the empty circles represent the delay versus gain for $D_p = 0$ but considering the SRS for $P_0 = 1, \ldots 5$ W; the single realizations for $D_p = 0.025\,\mathrm{ps}/\sqrt{\mathrm{km}}$ and with SRS are represented by the dots. The dashed line joins the mean gain-delay obtained by averaging the gain and the delay over the ensemble at the same P_0.

In conclusion, the SRS seriously affects the gain and the delay is also modified. If random birefringence is also taken into account a reduction with respect to the gain for $D_p = 0$ is observed. Differently from what occurred for small D_p but with no SRS (previous section), the curve that joins the mean gain-delay is not overlapped to the curve for $D_p = 0$ but is slightly shifted towards the lower values of gain, indicating an interaction between the random birefringence and the SRS.

V. Conclusion

An exact expression for the delay of slow light in NB-OPA not affected by random birefringence has been presented. The formula was confirmed by numerical simulations and enabled the exploration of the fiber parameter space without the need for lengthy numerical integrations. It also showed that the maximum achievable delay depends only on the fiber dispersion properties and the pump detuning from the zero dispersion wavelength. Then, the effects of the random birefringence

$$\int_0^L \mathrm{Im}[g_s(z)]dz = -\frac{1}{2}L(2\gamma P_0 + \Delta k) + \arctan\left[\frac{(2\gamma P_0 + \Delta k)\tanh\left[\frac{1}{2}L\sqrt{-\Delta k}\sqrt{4\gamma P_0 + \Delta k}\right]}{\sqrt{-\Delta k}\sqrt{4\gamma P_0 + \Delta k}}\right] \tag{8}$$

$$\begin{aligned}\Delta T(\omega) =& 2\gamma^2 P_0^2\left(6k_2 + k_4(\omega-\omega_p)^2\right)(\omega-\omega_p)\cosh\left[\frac{1}{2}L\sqrt{-\Delta k}\sqrt{\Delta k + 4\gamma P_0}\right] \\ &\times \frac{2\sqrt{-\Delta k}\sinh\left[\frac{1}{2}L\sqrt{-\Delta k}\sqrt{\Delta k + 4\gamma P_0}\right] + L\Delta k\cosh\left[\frac{1}{2}L\sqrt{-\Delta k}\sqrt{\Delta k + 4\gamma P_0}\right]\sqrt{\Delta k + 4\gamma P_0}}{3\Delta k\sqrt{\Delta k + 4\gamma P_0}\left(\Delta k^2 + 4\gamma P_0\Delta k + 2\gamma^2 P_0^2 - 2\gamma^2 P_0^2\cosh\left[L\sqrt{-\Delta k}\sqrt{\Delta k + 4\gamma P_0}\right]\right)}\end{aligned} \tag{9}$$

were also studied. For small random birefringence, the mean gain reduction is mainly due to the loss of alignment, which translates into an equivalent delay reduction, thus following the delay versus gain curve with no birefringence. For large random birefringence, severe pulse distortion occurs and the delay decreases faster than the gain. Moreover, a strong random birefringence causes a large uncertainty in the delay. This effect severely limits the reliability of NB-OPA as a slow and fast light device. Finally, the effects of the SRS have been also included: the SRS increases the attainable delay.

APPENDIX
CALCULATION OF THE DELAY OVER THE ENTIRE OPA GAIN BANDWIDTH

As shown in [2], [18] the scalar formulation of the NLSEs in the undepleted pump regime, yields exact analytical solutions for the pump, signal and idler waves. From the expression of the complex gain coefficient, $g_s(z)$, defined in [2], by integrating from 0 to L, it is straightforward to calculate (8), shown at the bottom of the previous page. Then, by differentiating (8) with respect to the optical frequency and for $-4\gamma P_0 < \Delta k < 0$, the exact delay is given by (9), shown at the bottom of the previous page, where we stress that $\Delta k = \Delta k(\omega)$. Equation (4) is calculated from (9), by assuming the phase-matching condition $\Delta k = -2\gamma P_0$ together with $\Delta k = k_2 (\omega - \omega_p)^2 + k_4 (\omega - \omega_p)^4/12$.

REFERENCES

[1] M. Marhic, K.-Y. Wong, and L. Kazovsky, "Wide-band tuning of the gain spectra of one-pump fiber optical parametric amplifiers," *IEEE J. Sel. Topics Quantum Electron.*, vol. 10, no. 5, pp. 1133–1141, Sep. –Oct. 2004.

[2] D. Dahan and G. Eisenstein, "Tunable all optical delay via slow and fast light propagation in a Raman assisted fiber optical parametric amplifier: A route to all optical buffering," *Opt. Exp.*, vol. 13, no. 16, pp. 6234–6249, Aug. 2005.

[3] E. Shumakher, A. Willinger, R. Blit, D. Dahan, and G. Eisenstein, "Low distortion propagation of high bit rate data streams in a slow light system based on narrow band Raman assisted parametric amplification in optical fibers," in *Tech. Digest Slow and Fast Light Topical Meeting (Paper Wb5)*, Washigton, DC, 2006.

[4] E. Shumakher, A. Willinger, R. Blit, D. Dahan, and G. Eisenstein, "Large tunable delay with low distortion of 10 Gbit/s data in a slow light system based on narrow band fiber parametric amplification," *Opt. Exp.*, vol. 14, no. 19, pp. 8540–8545, Sep. 2006.

[5] G. Eisenstein, A. Willinger, and E. Shumakher, "The effect of polarization mode dispersion on gain and delay spectra of Raman assisted narrow band fiber parametric amplifiers," in *Proc. 33rd Eur. Conf. Exhibition on Opt. Commun.*, Berlin, Sep. 16–20, 2007, no. 10.1.6 (GER).

[6] A. Willinger, E. Shumakher, and G. Eisenstein, "On the role of polarization and Raman assisted phase matching in narrow band fiber parametric amplifiers," *J. Lightwave Technol.*, to be published.

[7] E. Bettini, A. Galtarossa, L. Palmieri, M. Santagiustina, L. Schenato, and C. Someda, "Optical parametric amplification for slow light in random birefringence fibers," in *Proc. Photonics in Switching*, 2007, pp. 47–48.

[8] L. Schenato, M. Santagiustina, and C. G. Someda, "Narrow band optical parametric amplification for slow light in randomly birefringent fibers," in *Tech. Digest Optical Fiber Conf.'08*, 2008, vol. JThA3.

[9] E. Shumakher, A. Willinger, and G. Eisenstein, "Fundamental limits and recent advances in slow and fast light systems based on optical parametric processes in fibers," in *Proc. 9th Int. Conf. Transparent Optical Networks ICTON'07*, Jul. 1–5, 2007, vol. 1, pp. 262–265.

[10] Q. Lin and G. P. Agrawal, "Effects of polarization-mode dispersion on fiber-based parametric amplification and wavelength conversion," *Opt. Lett.*, vol. 29, no. 10, pp. 114–116, Oct. 2004.

[11] S. Trillo and S. Wabnitz, "Parametric and Raman amplification in birefringent fibers," *J. Opt. Soc. Amer. B.*, vol. 9, no. 7, pp. 1061–1082, Jul. 1992.

[12] R. Stolen and J. Bjorkholm, "Parametric amplification and frequency conversion in optical fibers," *IEEE J. Quantum Electron.*, vol. QE-18, no. 7, pp. 1062–1072, 1982.

[13] M. E. Marhic, N. Kagi, T.-K. Chiang, and L. G. Kazovsky, "Broadband fiber optical parametric amplifiers," *Opt. Lett.*, vol. 21, no. 8, p. 573, Aug. 1996.

[14] Q. Lin and G. P. Agrawal, "Effects of polarization-mode dispersion on cross-phase modulation in dispersion-managed wavelength division multiplexed systems," *J. Lightwave Technol.*, vol. 22, no. 4, pp. 977–987, Apr. 2004.

[15] A. Galtarossa and C. R. Menyuk, *Polarization Mode Dispersion*. New York: Springer, 2005.

[16] R. L. Smith, "The velocities of light," *Amer. J. Phys.*, vol. 38, no. 8, pp. 978–984, Aug. 1970.

[17] A. S. Y. Hsieh, G. K. L. Wong, S. Murdoch, S. G. Coen, F. Vanholsbeeck, R. Leonhardt, and J. D. Harvey, "Combined effect of Raman and parametric gain on single-pump parametric amplifiers," *Opt. Exp.*, vol. 15, no. 13, pp. 8104–8114, Jun. 2007.

[18] M.-C. Ho, K. Uesaka, M. Marhic, Y. Akasaka, and L. Kazovsky, "200-nm-bandwidth fiber optical amplifier combining parametric and raman gain," *J. Lightwave Technol*, vol. 19, no. 7, pp. 977–981, Jul. 2001.